

Shadow removal method for phase-shifting profilometry

LEI LU,¹ JIANGTAO XI,^{1,*} YANGUANG YU,¹ QINGHUA GUO,¹ YONGKAI YIN,^{1,2} AND LIMEI SONG³

¹School of Electrical Computer and Telecommunications Engineering, University of Wollongong, Wollongong, NSW 2522, Australia

²Key Laboratory of Optoelectronic Devices and Systems of Ministry of Education and Guangdong Province, College of Optoelectronic Engineering, Shenzhen University, Shenzhen 518060, China

³Computer Technic and Automatization College, Tianjin Polytechnic University, Tianjin, 300160, China

*Corresponding author: jiangtao@uow.edu.au

Received 31 March 2015; revised 29 May 2015; accepted 9 June 2015; posted 9 June 2015 (Doc. ID 237259); published 29 June 2015

In a typical phase-shifting profilometry system for the three-dimensional (3D) shape measurement, shadows often exist in the captured images as the camera and projector probe the object from different directions. The shadow areas do not reflect the fringe patterns which will cause errors in the measurement results. This paper proposed a new method to remove the shadow areas from taking part in the 3D measurement. With the system calibrated and the object reconstructed, the 3D results are mapped on a point-by-point basis into the corresponding positions on the digital micro-mirror device (DMD) of the projector. A set of roles are presented to detect the shadow points based on their mapped positions on the DMD plane. Experimental results are presented to verify the effectiveness of the proposed method. © 2015 Optical Society of America

OCIS codes: (120.6650) Surface measurements, figure; (100.2650) Fringe analysis; (120.5050) Phase measurement; (050.5080) Phase shift.

<http://dx.doi.org/10.1364/AO.54.006059>

1. INTRODUCTION

Phase-shifting profilometry (PSP) has been considered as an effective technology for nondestructive, high accuracy and high speed 3D shape measurement [1,2]. With PSP, a set of phase-shifted sinusoidal fringe pattern is casted onto the surface of the object, and their reflections are captured by a camera from a different angle. However, for some object shapes, the fringe patterns may not cover the entire surface, leaving areas of shadow on the acquired images. As these shadow areas do not carry the information associated with the object surface, significant error will occur in the results of the 3D reconstruction.

Several methods have been proposed to remedy the influence of the invalid points in the captured fringe patterns, including these from the shadow areas. Skydan *et al.* [3] used multiple projectors to probe the object from different angles to obtain a shadow-free surface reconstruction. However, the cost of the hardware will be increased significantly. Moreover, the typical PSP measurement system only requires one projector. Zhang [4] proposed to employ the Gaussian filter to smooth the fringe pattern, and then identify the invalid points using the monotonicity characteristic of the unwrapped phase map. However, although the Gaussian filter reduces the phase noise, it also introduces distortion to the details of the object surface. Chen *et al.* [5] proposed a method to identify the invalid points

by applying a threshold to the least-squares fitting errors in temporal phase unwrapping. However, in the presence of noise, not all invalid points can be identified as some invalid points also have the small least-squares fitting errors [6]. The data modulation and the intensity modulation of the fringe patterns are also employed to remove the shadow area [7–9], but there is not an effective way to determine the value of the threshold required by the methods.

This paper proposed a new method to eliminate the influence of the shadow areas in PSP. In particular, the paper considers the case that, the whole fringe pattern casted by the projector can be reflected by the object surface and are captured by the camera, but parts of the surface are not covered by the projected fringe pattern, leaving them as shadow areas in the captured image. The points in the shadow areas are invalid for 3D reconstruction and hence should be removed to avoid errors. The idea is as follows. First, the 3D reconstruction is carried out using the PSP method presented in [10], where the 3D shape is obtained based on the relationship among a point on the object surface, the corresponding point on the image captured by the camera, and a point on the fringe pattern projected by the projector. Due to the existence of shadows, the 3D data obtained contain errors. Then, using the above relationship, the 3D data are mapped into the DMD plane of the

projector on a point-by-point basis. At last, the shadow points are detected based on the mapped positions on the DMD plane.

The rest of this paper is organized as follows. In Section 2, the relationship between the world coordinate system, the camera coordinate system, and the projector coordinate system are given, and the principle of the 3D reconstruction described in [10] is presented. The proposed method is presented in Section 3. The experimental results are shown in Section 4, and Section 5 concludes this paper.

2. PRINCIPLE OF THE 3D RECONSTRUCTION

Figure 1 shows the schematic diagram of the measurement system presented in [10], which involves three coordinate systems, including the projector coordinate system ($O^p; u^p, v^p$), the camera coordinate system ($O^c; u^c, v^c$), and the world coordinate system ($O^w; x^w, y^w, z^w$). A point (x^w, y^w, z^w) on the object surface corresponds to the positions at the other two coordinates by the following relationship [10]:

$$\begin{cases} s_c [u^c, v^c, 1]^T = \mathbf{A}^c \mathbf{R}^c \mathbf{T}^c [x^w, y^w, z^w, 1]^T \\ s_p [u^p, v^p, 1]^T = \mathbf{A}^p \mathbf{R}^p \mathbf{T}^p [x^w, y^w, z^w, 1]^T \end{cases} \quad (1)$$

where \mathbf{A}^c and \mathbf{A}^p are the intrinsic parameter matrixes for the camera and projector respectively; $(\mathbf{R}^c, \mathbf{T}^c)$ and $(\mathbf{R}^p, \mathbf{T}^p)$ are the extrinsic parameter matrixes for the camera and projector respectively. s_c and s_p are the scale factors, which are functions of (x^w, y^w, z^w) . The intrinsic and extrinsic parameters can be obtained through the calibration of the system. In Eq. (1), there are four equations and five unknown parameters (x^w, y^w, z^w, u^p, v^p). Therefore, in order to obtain the height distribution of the object (x^w, y^w, z^w), an additional constraint can be introduced by the corresponding relationship between the

(u^c, v^c) and (u^p, v^p) , based on the phase relationship obtained by PSP.

For the N-step PSP, images with phase-shifted fringes vertical to the direction u^p are projected by the projector and can be expressed as

$$d_n^p(u^p, v^p) = a + b \cos \left(\Phi^p(u^p, v^p) + \frac{2\pi(n-1)}{N} \right), \quad (2)$$

where $n = 1, 2, 3, \dots, N$; $\Phi^p(u^p, v^p) = 2\pi f_0 u^p$ is the designed absolute phase map in the projector, and f_0 is the frequency of the fringe pattern designed in the projector; a and b can be set in the computer to adjust the intensity of the fringe patterns. Then, the fringe patterns are captured by the camera and can be expressed as

$$d_n^c(u^c, v^c) = A(u^c, v^c) + B(u^c, v^c) \cos \left(\phi^c(u^c, v^c) + \frac{2\pi(n-1)}{N} \right), \quad (3)$$

where

$$A(u^c, v^c) = c[r(u^c, v^c)a + d^a(u^c, v^c)], \quad (4)$$

and

$$B(u^c, v^c) = cr(u^c, v^c)b. \quad (5)$$

$A(u^c, v^c)$ is the average intensity, and $B(u^c, v^c)$ is the intensity modulation of the sinusoidal fringe patterns; c denotes the sensitivity to the light of the camera; $r(u^c, v^c)$ is the reflectivity of the object surface; $d^a(u^c, v^c)$ is the ambient light. When $N \geq 3$, $A(u^c, v^c)$, $B(u^c, v^c)$ and $\phi^c(u^c, v^c)$ can be obtained by the following,

$$A(u^c, v^c) = \frac{1}{N} \sum_{n=1}^N d_n^c(u^c, v^c), \quad (6)$$

$$B(u^c, v^c) = \frac{2}{N} \sqrt{\left[\sum_{n=1}^N d_n^c(u^c, v^c) \sin \left(\frac{2\pi n}{N} \right) \right]^2 + \left[\sum_{n=1}^N d_n^c(u^c, v^c) \cos \left(\frac{2\pi n}{N} \right) \right]^2}, \quad (7)$$

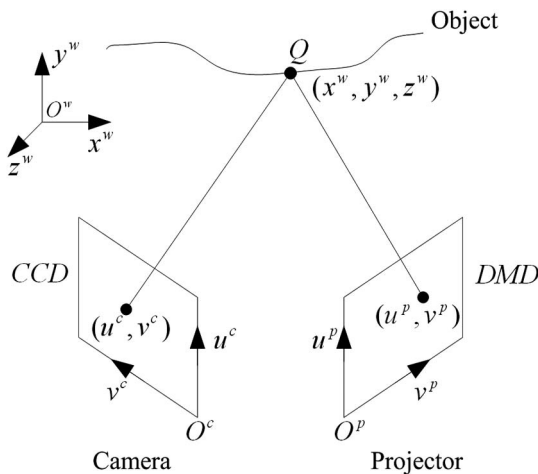


Fig. 1. Schematic diagram of the measurement system.

$$\phi^c(u^c, v^c) = \arctan \frac{-\sum_{n=1}^N d_n^c(u^c, v^c) \sin 2\pi n/N}{\sum_{n=1}^N d_n^c(u^c, v^c) \cos 2\pi n/N}. \quad (8)$$

Define

$$\gamma(u^c, v^c) = \frac{B(u^c, v^c)}{A(u^c, v^c)}, \quad (9)$$

where $0 < \gamma(u^c, v^c) < 1$ is the data modulation, and it can be used to describe the quality of the fringe pattern in terms of signal to noise ratio [11,12]. The higher of the $\gamma(u^c, v^c)$, the better of the quality.

With the fringe patterns captured by the camera, the wrapped phase map $\phi^c(u^c, v^c)$ can be obtained by Eq. (8), which is then unwrapped to yield the absolute phase map $\Phi^c(u^c, v^c)$. Note that in the phase map $\Phi^p(u^p, v^p)$, the absolute phase values are constant with respect to v^p for the same u^p .

Therefore, for a specific point (u^c, v^c) , a line along u^p on the DMD can be found based on $\Phi^p(u^p, v^p) = \Phi^c(u^c, v^c)$.

From Eq. (1), three linear equations can be obtained as the following,

$$\begin{cases} f_1(x^w, y^w, z^w, u^c) = 0 \\ f_2(x^w, y^w, z^w, v^c) = 0, \\ f_3(x^w, y^w, z^w, u^p) = 0 \end{cases} \quad (10)$$

where (u^c, v^c, u^p) are known. Therefore, (x^w, y^w, z^w) can be determined by solving Eq. (10).

3. PROPOSED METHOD

The object is reconstructed with the process described in Section 2. However, in practice, there are shadows existing in the captured images. The shadows do not contain the information of the projected fringe patterns. When Eq. (8) is applied to the points in the shadow area, errors will be introduced in the phase value. The incorrect phase value will be corresponded to an invalid u^p in the DMD plane, leading to the errors in the reconstruction of the object.

A. Causes of Shadow

In order to remove the points in the shadow area, the reason causing the shadow in the PSP system should be analyzed. In the schematic diagram of the PSP system shown in Fig. 2, the scope of the camera and the projector is $E_c R_1 R_6$ and $E_p R_1 R_6$, respectively. The light beam $E_p P R_5$ emitted from the projector is projected onto the point R_5 through point P on the object. Due to the sharp change in the height of the object at point P , a shadow area $PR_3 R_5$ will be formed. The camera captures the fringe patterns in another direction, and it can observe point R_4 through point P . It is apparent that the shadow area $PR_4 R_5$ will be captured by the camera, which does not contain the information of the projected fringe patterns.

B. Identification of the Points in Shadow

We propose to identify the points in shadow by verifying whether the captured fringe patterns are projected from the DMD plane or not. In order to do this, the whole image captured by the camera can be divided into two types of area, namely the fringe pattern area and shadow area. Assuming the camera can see all the areas on the object surface illuminated by the projector (as shown in Fig. 2), the fringe pattern area on the

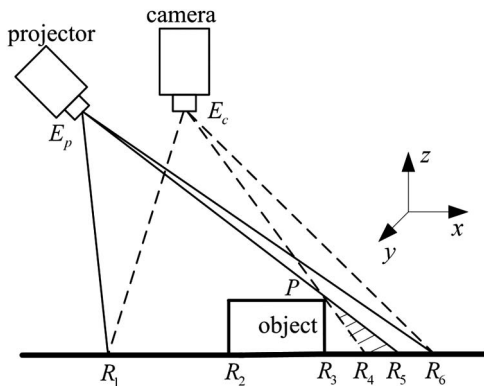


Fig. 2. Reason causes shadow in the PSP system.

camera image will cover the whole fringe pattern projected. While correct 3D reconstruction can be obtained from the fringe pattern area, measurement error occurs due to the shadow areas. If we map all the points of the reconstructed result (include the fringe pattern area and shadow area) to the DMD plane using Eq. (1), the points from the fringe pattern area will cover all the points on the DMD plane. In contrast, the mapped points from the shadow area may be outside or inside the boundary of the DMD. We will make use of the positions associated with the mapped points to detect the shadow areas. The details of the proposed approach are described below.

If a point is mapped outside the DMD boundary (Type1), it will be detected as the shadow point. This is because the entire fringe pattern is reflected by the object surface, and hence if a 3D point is valid, its corresponding mapped point on DMD must be within the dimension of the fringe pattern, i.e., the boundary of the DMD.

If a mapped point has a unique position within the boundary of DMD (Type 2), the point will be detected as a valid point. This is also because the entire fringe pattern is reflected by the object surface, implying that any point on the pattern is utilized for 3D reconstruction, which must correspond to a valid 3D point. Hence, if the mapped point is unique on the DMD, the 3D point must be valid.

3D points in the shadow area may also be mapped to the points within the boundary of the DMD, but in this case these points must coincide with others, because the valid 3D data must cover the entire DMD. Therefore, for the mapped points that fall within the boundary of DMD but are not unique (Type 3), one must be valid and the remaining from the shadow ones. In this case, decision needs to be made to identify the valid one.

For these Type 3 points, we propose to use the data modulation $\gamma(u^c, v^c)$ to identify the shadow [8,13]. The shadow areas usually only contain the ambient light $d^a(u^c, v^c)$ and hence from Eq. (6) and Eq. (7) we have

$$A(u^c, v^c) = d^a(u^c, v^c), \quad (11)$$

and

$$B(u^c, v^c) = 0. \quad (12)$$

From the expression of the data modulation $\gamma(u^c, v^c)$ described in Eq. (9), we can see that $\gamma(u^c, v^c) = 0$ or should be very small if not zero for the points in shadow.

In contrast, for the valid points reflecting the fringe patterns, submit Eq. (4) and Eq. (5) into Eq. (9), and we have

$$\gamma(u^c, v^c) = \frac{r(u^c, v^c)b}{r(u^c, v^c)a + d^a(u^c, v^c)}. \quad (13)$$

In practice, $a = b$ is usually used in the projector in order to make full use of the intensity range, and the ambient light $d^a(u^c, v^c)$ is much smaller than the a and b . Therefore, when the reflectivity $r(u^c, v^c)$ is not too small, the $\gamma(u^c, v^c)$ should exhibit larger values in the fringe pattern areas than the ones in the shadow areas.

Consequently, when multiple points are overlapping in the DMD plane, the one with the biggest $\gamma(u^c, v^c)$ can be identified as the valid point and the rest as the invalid points from the

shadow. Different from other methods employing the data modulation to remove the shadow, a threshold is not required in the proposed method, resulting in a more flexible and robust algorithm.

In summary, the proposed method can be implemented by the following steps.

Step 1: Calibrate the measurement system and reconstruct the object by Eq. (10).

Step 2: Map all the points of the reconstructed result to the DMD plane of the projector.

Step 3: If the coordinate of the mapped point exceeds the valid range of the DMD plane (Type 1), it is shown as the invalid point from the shadow area directly.

Step 4: If the coordinate of the mapped point falls in the valid range of the DMD plane uniquely (Type 2), it is demonstrated as the valid point on the object surface.

Step 5: If multiple points are mapped to the same coordinate in the DMD plane (Type 3), use the data modulation $\gamma(u^c, v^c)$

to identify the points in the shadow. The point with the biggest $\gamma(u^c, v^c)$ is the valid point and the others are identified as the shadow.

4. EXPERIMENTS AND RESULTS

In order to verify the proposed algorithm, a plaster pyramid model shown in Fig. 3(a) is reconstructed in the experiments. As the proposed method requires all the projected fringe patterns on the object that can be captured by the camera, the object must be put on the position of left side or right side of the camera and the projector (on right side as shown in Fig. 2) instead of between the camera and projector. A three-step PSP is utilized to reconstruct the object, and Fig. 3(b) is one of the captured fringe patterns. It is apparent that the shadow area exists in the captured fringe pattern of the object. In the experiments, the absolute phase map is obtained with the help of six Gray-code patterns. The decoded Gray-code value is

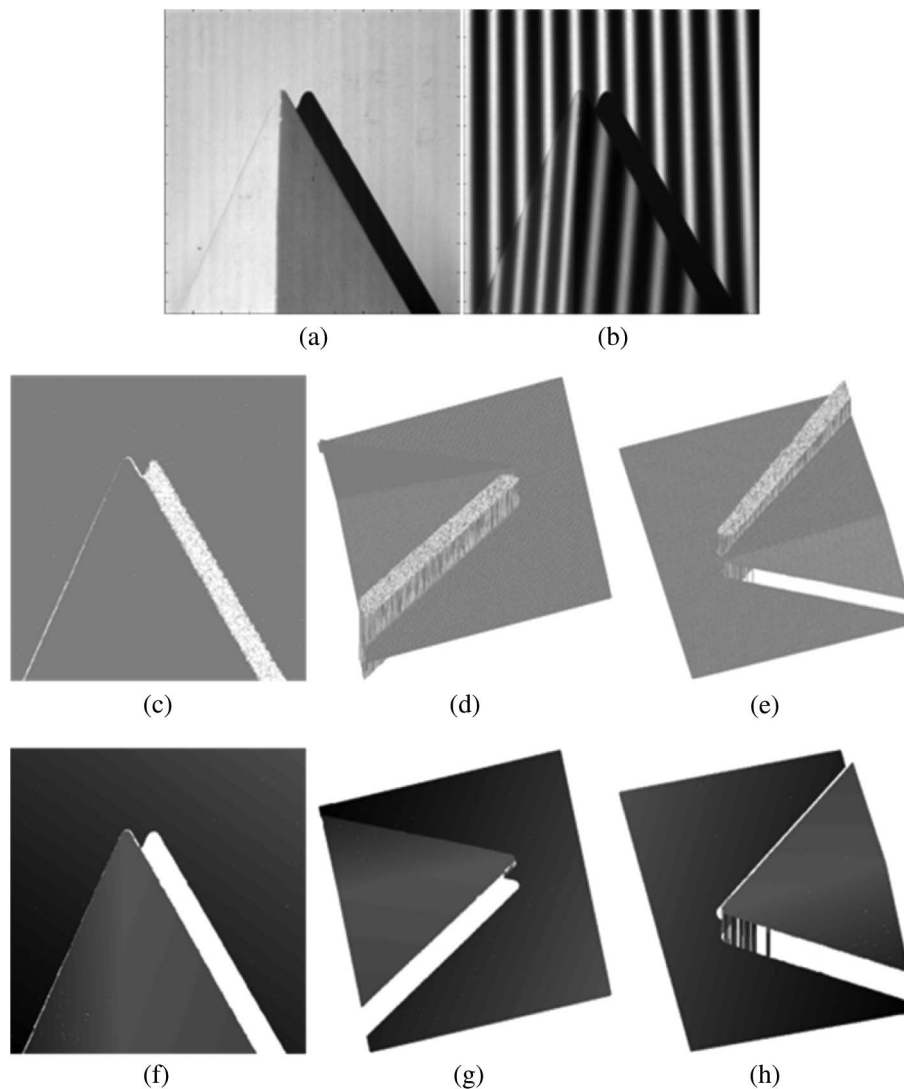


Fig. 3. (a) The front view of the measured pyramid; (b) One of the captured fringe patterns for the measured pyramid; (c)–(e) The front view, the right side and the left side of the reconstructed result by PSP; (f)–(h) The front view, the right side and the left side of the reconstructed result from the proposed method.

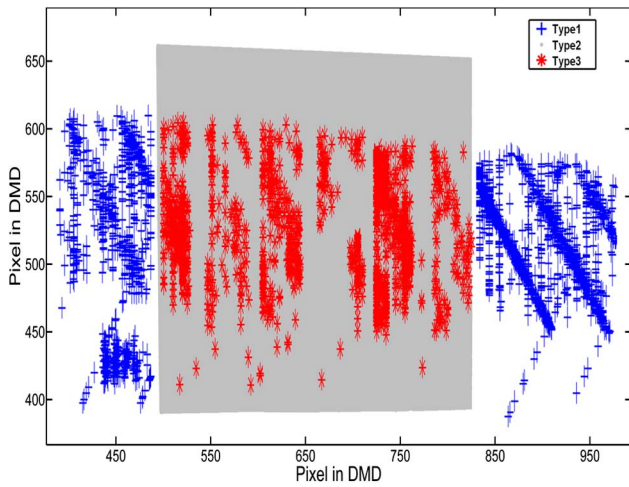


Fig. 4. Distribution of the mapped points in DMD for experiment 2.

used as the index of the period of the fringe patterns. Due to the existence of the shadow, the decoded Gray-code is also not correct in the shadow area, leading to the loss of monotonicity associated with the absolute phase map.

In the first experiment, the object is reconstructed by the three-step PSP directly. The reconstructed result is shown in Figs. 3(c)–3(e). It is apparent that, the result of the points on the object matches the expectations of the PSP, but the points in the shadow area are reconstructed with errors.

In the second experiment, the proposed method is applied on the same fringe patterns used in the above experiment. The reconstructed results (x^w, y^w, z^w) obtained in the first experiment are mapped to the DMD plane by calculating (u^p, v^p) with Eq. (1). As shown in Fig. 4, the gray area is the captured fringe pattern area in DMD (Type 2). Please note that in practice, the boundary of the fringe pattern area in DMD can be obtained by calibration. Some points are outside of the boundary of the fringe pattern area in DMD, which are considered as Type 1. We also observed that some points are overlapped

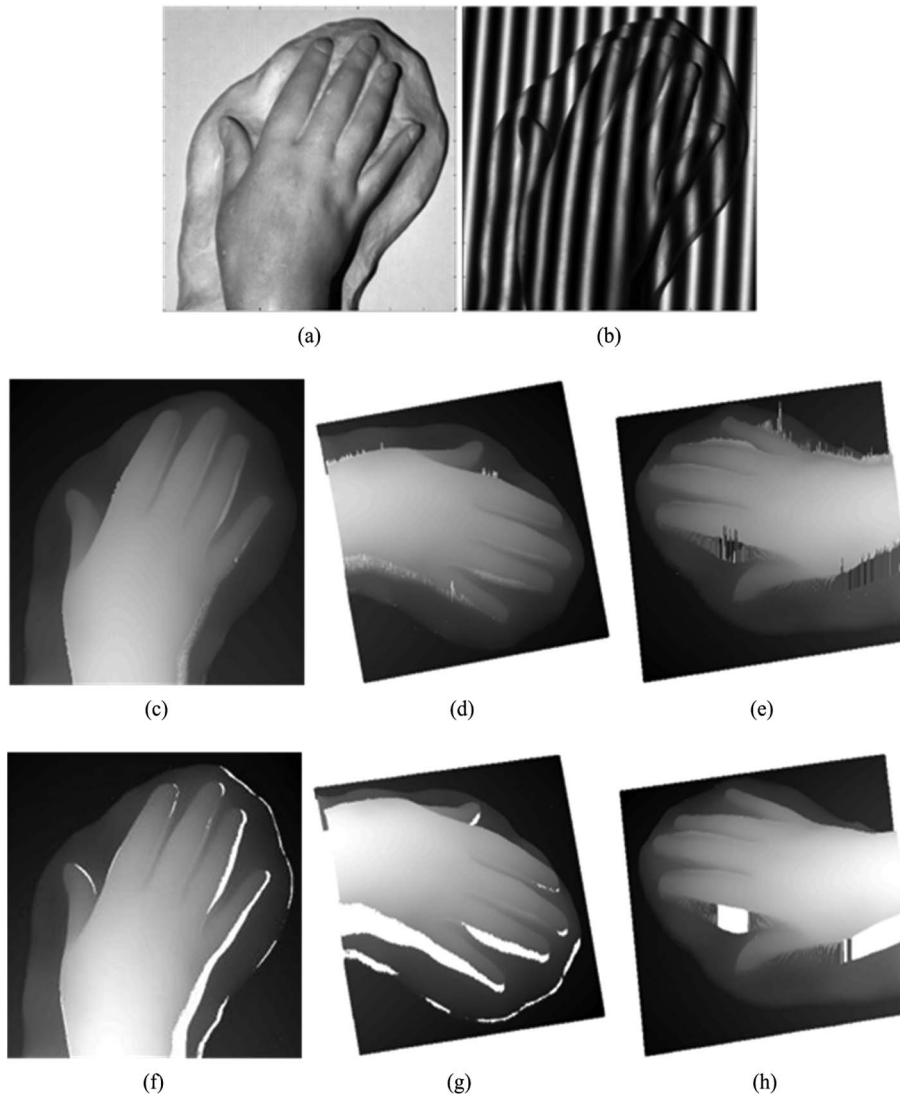


Fig. 5. (a) The front view of the measured hand model; (b) One of the captured fringe patterns for the measured hand model; (c)–(e) The front view, the right side and the left side of the reconstructed result by PSP; (f)–(h) The front view, the right side and the left side of the reconstructed result by the proposed method.

within the boundary, and hence data modulation $\gamma(u^c, v^c)$ is used to identify the Type 3 points. With the proposed method, the measurement results are obtained in Figs. 3(f)–3(h), showing that all the erroneous points in the shadow area are completely removed, leaving only the valid 3D measurement results.

Then, a plaster hand model with complex shape shown in Fig. 5(a) is measured in the experiment. Figure 5(b) is one of the captured fringe pattern of the object. The shadow area not only exists on the right side of the object, but also exists between the fingers.

Figures 5(c)–5(e) show the reconstructed result when the three-step PSP is employed, showing obvious errors in the shadow areas.

Then, the proposed method is applied and the reconstructed result is shown in Figs. 5(f)–5(h). Compared with the result shown in Fig. 5(c)–5(e), the points in the shadow area are removed clearly and significant improvement is achieved.

5. CONCLUSION

In summary, a new approach to remove the points in the shadow area based on the PSP is presented in this paper. The proposed method removes the shadow by identifying whether the captured fringe pattern is projected from the projector or not. As a threshold is not required, the proposed method is more flexible and performs better than existing methods in the practice. Moreover, the proposed method does not involve such operations as the Gaussian filter and the least-square fitting, hence is computationally efficient. The performance of the proposed method has been verified by the experiments.

Funding. Natural Science Foundation of China (61405122).

REFERENCES

1. S. Zhang, "Recent progresses on real-time 3-D shape measurement using digital fringe projection techniques," *Opt. Lasers Eng.* **48**, 149–158 (2010).
2. S. S. Gorthi and P. Rastogi, "Fringe projection techniques: Whither we are?" *Opt. Lasers Eng.* **48**, 133–140 (2010).
3. O. A. Skydan, M. J. Lalor, and D. R. Burton, "Using coloured structured light in 3-D surface measurement," *Opt. Lasers Eng.* **43**, 801–814 (2005).
4. S. Zhang, "Phase unwrapping error reduction framework for a multiple-wavelength phase-shifting algorithm," *Opt. Eng.* **48**, 105601 (2009).
5. F. Chen, X. Su, and L. Xiang, "Analysis and identification of phase error in phase measuring profilometry," *Opt. Express* **18**, 11300–11307 (2010).
6. L. Huang and A. K. Asundi, "Phase invalidity identification framework with the temporal phase unwrapping method," *Meas. Sci. Technol.* **22**, 035304 (2011).
7. S. Zhang, "Composite phase-shifting algorithm for absolute phase measurement," *Opt. Lasers Eng.* **50**, 1538–1541 (2012).
8. D. L. Lau, K. Liu, and L. G. Hassebrook, "Real-time three-dimensional shape measurement of moving objects without edge errors by time-synchronized structured illumination," *Opt. Lett.* **35**, 2487–2489 (2010).
9. K. Zhong, Z. Li, Y. Shi, C. Wang, and Y. Lei, "Fast phase measurement profilometry for arbitrary shape objects without phase unwrapping," *Opt. Lasers Eng.* **51**, 1213–1222 (2013).
10. S. Zhang and P. Huang, "Novel method for structured light system calibration," *Opt. Eng.* **45**, 083601 (2006).
11. S. Zhang and S. Yau, "High-resolution, real-time 3D absolute coordinate measurement based on a phase-shifting method," *Opt. Express* **14**, 2644–2649 (2006).
12. P. S. Huang and S. Zhang, "Fast three-step phase-shifting algorithm," *Appl. Opt.* **45**, 5086–5091 (2006).
13. X. Su, G. von Bally, and D. Vukicevic, "Phase-stepping grating profilometry: Utilization of intensity modulation analysis in complex objects evaluation," *Opt. Commun.* **98**, 141–150 (1993).